RSC Advances

PAPER

View Article Online
View Journal | View Issue

Cite this: *RSC Adv.*, 2016, **6**, 61386

Highly transparent silver nanowire–polyimide electrode as a snow-cleaning device†

Chin-Yen Chou,‡ Huan-Shen Liu‡ and Guey-Sheng Liou*

Received 17th May 2016
Accepted 17th June 2016

DOI: 10.1039/c6ra12828a

www.rsc.org/advances

In this study, highly transparent and flexible electrodes were prepared by the hybrid technique of silver nanowires (AgNWs) and colorless high performance polyimides (PIs). By introducing AgNWs with a high aspect ratio of 600, the novel flexible AgNW–PI electrodes having figure of merit (FoM) value up to 260 could be obtained with a resistance of 3.6 Ω sq^{-1} and transmittance up to 70% at a 550 nm wavelength. Moreover, the PI binder effectively enhanced the adhesion between AgNWs and the PI substrate even after bending for 12 000 cycles and tape peeling for 1000 cycles, respectively. The obtained highly transparent and flexible AgNW electrodes could endure harsh working environments and post-processing by taking the thermal and chemical stability advantages of PIs. Furthermore, highly transparent AgNW–PI hybrid electrodes could be fabricated to demonstrate their feasibility as a snow-cleaning heater.

Introduction

With technology advancing, a great deal of electronic products have been developed rapidly. From a scientific point of view, a transparent and conductive electrode is inevitable for displaying and monitoring, and how to enhance the performance of an electrode with both high conductivity and transmittance is an essential issue. Although indium tin oxide (ITO) has occupied most of the market due to its excellent properties in combination with its electrical and optical behavior, its disadvantages including high cost and brittle property are crucial problems that need to be dealt with.[1] Therefore, some novel alternatives have attracted great attention such as carbon nanotubes (CNTs),[2] graphene,[3] and metallic nanowires.[4] However, the cost of the equipment and the high vacuum system required for continuous large-scale CVD production handicap the research field of CNTs or graphene.[5] Thus, metallic nanowires such as silver nanowire (AgNW), with excellent conductivity, ductility, and easy processing among the conducting materials, has become the most representative target.[4]

Before 2002, template-transferring[6] and electrodeposition[7] were popular methods for generating AgNWs. However, disadvantages, such as irregular morphology, low aspect ratio, and low yield, slow down the applicability of silver nanowires. Until 2002, Xia's group first proposed the polyol method to produce AgNWs bottom-up by a simple and large-scale way using poly(vinylpyrrolidone) (PVP) as a capping agent and ethylene glycol (EG) as a reductant to reduce the silver nitrate.[8] Thus, a lot of research that focused on growth theory and synthesis parameters has been performed to produce versatile metallic nanowires for high-tech applications. In order to highlight the advantages of AgNWs, the first AgNW–polymer (PET) hybrid flexible electrode was prepared by Coleman's group.[9] However, poor adhesion between AgNWs and the substrate handicaps practical application. Thus, how to improve the adhesion problem becomes an important issue. For example, Cui's group applied Teflon as an encapsulating material to stabilize AgNW networks on a flexible substrate,[10] using polymers as both the substrate and binder such as polydimethylsiloxane (PDMS),[11–17] polyacrylate,[18–20] polyurethane (PU),[21–23] poly(methyl methacrylate) (PMMA),[24,25] polycarbonate (PC),[26,27] polyvinyl alcohol (PVA),[28–30] and polyimide (PI),[31,32] which have joined the family of AgNW hybrid electrodes. In addition, there are many applications for AgNW–polymer transparent electrodes that have been reported such as solar cells,[33–36] LEDs,[37,38] touch screens,[39,40] heaters,[41–47] and electrochromic devices (ECDs).[48]

Although AgNW transparent electrodes based on polymeric substrates have developed extensively, the thermal stability of substrates was not emphasized until 2012. The requirement for thermal stability in AgNW–polymer hybrid systems was first indicated from Kim's group by introducing PI for the application of solar cell devices, and a FoM value around 180 of the resulting AgNW–PI electrodes was also achieved.[32] However, the cut-off wavelength of common polyimides adopted in the AgNW system was still high due to the coloration by charge transfer

Institute of Polymer Science and Engineering, National Taiwan University, Taipei, Taiwan 10617. E-mail: gsliou@ntu.edu.tw

† Electronic supplementary information (ESI) available: Experimental section; Table: solubility behavior, thermal properties, and optical properties of polyimides; Figure: TGA, AFM and SEM photos of synthesized polyimides, high aspect ratio AgNWs, and AgNWs–PI hybrid films. See DOI: 10.1039/c6ra12828a

‡ These authors contributed equally to this work.

complex (CTC) formation that results in a PI film with yellowish color and is insufficient for practical applications.

Therefore, it is necessary to highlight the advantages and potentials of high-performance polymers by appropriate structural design in order to fulfill higher requirements during working or processing. Herein, a thermally stable, organo-insoluble, and colorless polyimide with high transmittance was chosen as the binder in this study to increase chemical resistance and prevent AgNWs from peeling off. In addition, by introducing AgNWs with a higher aspect ratio into the polyimide system, both optical and electrical properties of the AgNW–PI hybrid electrodes could also be enhanced. To the best of our knowledge, this is the highest FoM value for AgNW–PI hybrid electrodes with not only low electrical resistance, excellent optical transparency, and high flexibility, but also high thermal stability and chemical resistance that could satisfy different kinds of solvent processing, annealing processes, and work as snow-cleaning heaters.

Experimental

Materials

Silver nitrate (99.85%, ACROS), polyvinylpyrrolidone (PVP) (MW = 1 300 000, Alfa Aesar), ethylene glycol (EG) (SHOWA), copper(II) chloride (98%, SHOWA), iron(III) chloride (97%, SHOWA) and organic solvents such as *N*,*N*-dimethylacetamide (DMAc) (TEDIA), *N*-methyl-2-pyrrolidinone (NMP) (TEDIA), *N*,*N*-dimethylformamide (DMF) (TEDIA), dimethyl sulfoxide (DMSO) (TEDIA), tetrahydrofuran (THF) (ECHO), and acetic acid (Scharlau) were purchased and used without purification. 4,4′-Biphthalic dianhydride (BPDA) (>97%, TCI) was purchased and purified by sublimation. 1,4-Cyclohexanediamine (CHDA) (99%, Acros) was purchased and purified by recrystallization in *n*-hexane and dried in a vacuum at room temperature for 24 hours. 2,2′-Bis-(trifluoromethyl)benzidine (TFMB) and 1,2,4,5-cyclohexanetetracarboxylic dianhydride (HPMDA) were supplied from the industrial technology research institute (ITRI) of Taiwan, and TFMB was purified by recrystallization in ethanol and water to obtain a white crystal, while HPMDA was dried in a vacuum oven at 120 °C for 6 hours.

Synthesis of silver nanowires

The AgNWs were prepared by the modified polyol process which adopts PVP as the capping agent and EG as the reductant to reduce silver nitrate.[49] Firstly, 50 mL of EG was added into a 250 mL three necked flask, and stirred at 140 °C for one hour under nitrogen atmosphere. At the same time, EG solutions mixed with $AgNO_3$ (0.094 M) and PVP (0.147 M) were prepared individually and placed at the room temperature. After preheating the EG for an hour, 400 μL of 4 mM copper(II) chloride/EG solution was added into the flask and stirred for 15 minutes, then the PVP/EG solution was added into the flask with the silver nitrate/EG solution injected (0.5 mL min^{-1}) at the same time. After reacting at 140 °C for 1.5 hour, the solution turned into a silver white suspension. The suspension was then washed with ethanol and separated by the centrifugation method (2000 rpm for 15 minutes, 6 times) to remove the supernatant which contained residual PVP and silver nanoparticles. Finally, the washed AgNWs were dispersed and stored in 50 mL of ethanol. The SEM morphology of synthesized AgNWs is summarized in Fig. S1.†

Synthesis of colorless polyimides

In this study, two kinds of colorless polyimides were synthesized including TFMBCH PI, which served as a substrate, and organo-insoluble CHDABP PI, used as a AgNW binder and protector. The chemical structures are shown in Scheme 1, and the synthetic processes are described as follows.

Transparent and colorless TFMBCH PI. The colorless polyimide TFMBCH PI was synthesized according to a conventional two-step method by thermal imidization as follows: 1.601 g (5 mmol) of TFMB was first dissolved in 7.0 mL of DMAc under nitrogen atmosphere, 1.121 g (5 mmol) of HPMDA was then added into the flask (30 wt% solid content) and kept stirring at room temperature for 72 hours to form poly(amic acid) (PAA). Finally, the PAA solution was casted on the glass and dried in a vacuum oven at room temperature for 6 hours, and the temperature was increased slowly to 300 °C, and then maintained for 2 hours to form the TFMBCH PI film. The obtained PI film could be dissolved in DMAc again.

Organo-insoluble CHDABP PI. The organo-insoluble CHDABP PI was synthesized according to the conventional two-step method by thermal imidization. 0.571 g (5 mmol) of CHDA was dissolved in 7.5 mL of DMAc at 70 °C under nitrogen atmosphere. The solution was cooled down to room temperature, and then 0.600 g (10 mmol) of acetic acid was slowly added. After 10 minutes, 1.471 g (5 mmol) of BPDA was added into the solution. The mixture was mechanically stirred for 48 hours at room temperature to form a PAA solution, then casted, and the temperature was slowly raised to 250 °C and maintained for 2 hours to obtain organo-insoluble CHDABP PI.

Fabrication of the AgNW–PI flexible transparent electrode

A schematic diagram of the fabrication procedure for the AgNW–PI hybrid electrode is depicted in Fig. 1. The various

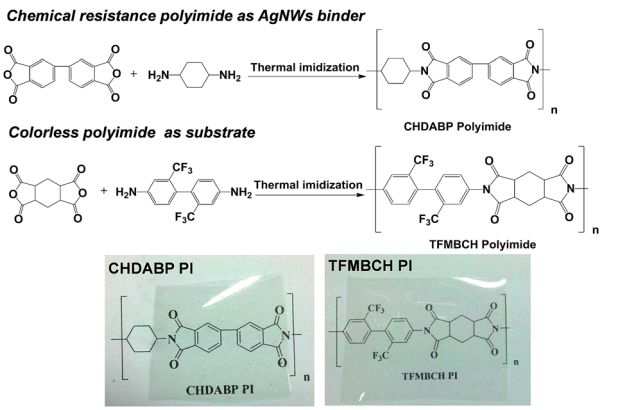

Scheme 1 The preparation of colorless polyimides CHDABP PI and TFMBCH PI.

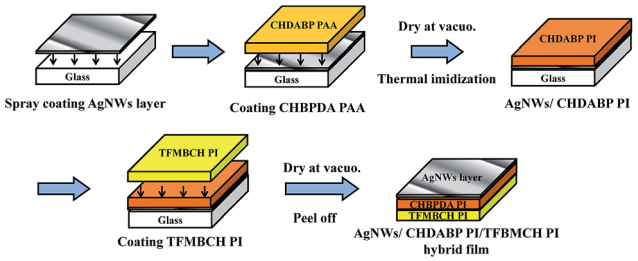

Fig. 1 Schematic diagram for the fabrication of AgNW–PI transparent and flexible electrode.

concentrations of the AgNW/ethanol solution was firstly spray-coated by an airbrush gun (nozzle diameter: 0.35 mm) on 5.0 × 5.0 cm^2 washed glass which was preheated at 120 °C on the hotplate. The back pressure was set at 15 psi with a spraying distance of 15 cm from the surface of the glass substrate. Next, the CHDABP PAA solution was spin coated on AgNW networks with the thickness controlled at 150 nm and baked at 100 °C for 5 min under nitrogen atmosphere. The temperature of the AgNW–CHDABP PAA hybrid film was raised slowly to 250 °C for 2 hours to imidize completely. Finally, the TFMBCH PI solution was rod casted onto the AgNW–CHDABP PI hybrid film. After drying in a vacuum oven, the AgNW–PI hybrid film was lifted off from the glass substrate and a flexible conductive layer was obtained on the other side, and the total thickness of the resulting hybrid films was controlled at around 20 μm.

Fabrication of AgNW–PI electrodes for snow-cleaning device

The preparation of the snow-cleaning device based on the AgNW–PI hybrid electrode is listed as follows. The prepared AgNW/ethanol solution (aspect ratio: 600) was first spray coated on a 5.0 × 5.0 cm^2 washed glass which was preheated to 120 °C. Next, the TFMBCH PI solution was drop casted on AgNW networks with the thickness controlled at 100 nm and baked in a vacuum oven at 150 °C for 1 hour. The resulting AgNW–PI hybrid electrode which exhibited a sheet resistance of 6.3 ± 0.5 Ω sq^{-1} and transmittance (T_{550nm}) of 76% was then covered with another glass and sealed by Kapton tape in order to simulate the condition of a windshield.

Characterization

Thermogravimetric analysis (TGA) using a TA instrument Q50 was used to measure the thermal stability of the polymers and hybrid films. Field emission scanning electron microscopy (FE-SEM, JEOL, JSM-6700F) was used to examine the surface morphology and microstructure of the AgNWs and hybrid films. UV-vis spectra of the polymers and hybrid films were recorded using a Hitachi U-4100 UV-vis-NIR spectrophotometer in the wavelength range of 400–800 nm. The resistance of the transparent electrodes was measured by the handheld LCR meter (Agilent U1732C). The sheet resistance was obtained by the four point probes (Keithlink Technology 2000) measured values which were multiplied by 4.532. The diameter of the probes is 100 μm and the space of each probe is 1.6 mm. The electrical thermometer (TES 1310 TKPE-K) was used to measure the temperature of the snow-cleaning device.

Results and discussion

Basic characterization

The polyimides of TFMBCH PI and CHDABP PI used in this study are depicted in Scheme 1. The basic properties such as thermal properties and solubility of these PIs are summarized in Tables S1, S2, and Fig. S2.† All the PIs showed outstanding thermal stability with T_d^5 and T_d^{10} up to 475 °C in both nitrogen and air conditions. Owing to the packing-disruptive moieties in the main chains of the polymer, the substrate TFMBCH PI and binder CHDABP PAA exhibited good solubility in common organic solvents such as DMAc and NMP. Thus, large scale processing of these two kinds of polyimides and precursors are easy to carry out by spin-coating or rod-casting. On the other hand, the CHDABP PI binder thermally imidized from the PAA precursor revealed excellent chemical resistance to common organic solvents. Due to the organic-insoluble CHDABP PI acting as the AgNW binder, the obtained AgNW–PI electrodes could enhance the potential to endure another post-processing. The optical properties are tabulated in Table S3.† Because the charge-transfer effect on PI was suppressed by the introduction of high electronegative bulky fluorine atoms and adoption of aliphatic monomers, these PI films exhibited highly colorless and optical transparency.

Properties of flexible and transparent AgNW–polyimide electrodes

The electrical and optical properties of these flexible and transparent AgNW–PI electrodes are summarized in Fig. 2. The

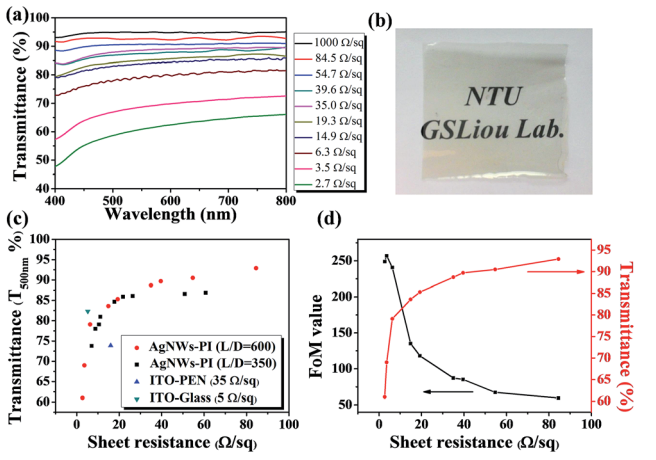

Fig. 2 The electrical and optical behavior of the prepared AgNW–PI flexible and transparent electrodes. (a) UV-vis transmittance spectra of the obtained electrodes with various amounts of AgNWs coated on glass (the transmittance based on the PI substrate as a reference), (b) photo for demonstration of the AgNW–PI hybrid film with the highest FoM value, (c) transmittance at 550 nm (T_{550nm}) plotted with sheet resistance (Ω sq^{-1}) of AgNW–PI hybrid films, and (d) FOM value plotted with sheet resistance and transmittance (T_{550nm}) of the flexible electrodes.

optical transparency of AgNW–PI hybrid films with different amounts of AgNWs measured by UV-vis spectra is presented in Fig. 2a. Owing to the nano-scale diameter of AgNWs, most of the visible light could pass through the gap of the networks so that the AgNW–PI hybrid films exhibited high transparency. The more AgNW content in the PI film, the greater the probability that passing light will be blocked, which is a dilemma in the relationship between the optical transparency and conductivity of AgNW–PI hybrid films. Therefore, optimization of the AgNW amount is an important parameter to produce hybrid electrodes with an excellent balance between transparency and conductivity. The sheet resistance plotted with transmittance (PI substrate served as background) at a 550 nm wavelength with different amounts of AgNWs is shown in Fig. 2b. Because the high aspect ratio of AgNWs (600) was used to fabricate the AgNW–PI hybrid films, the obtained electrodes exhibited an advance of both transmittance and conductivity compared with the low aspect ratio (350) reported by previous literature.[48]

The figure of merit (FoM) is a representative quantity used to evaluate the performance of transparent conductors,[9,50] and the FoM for transparent electrodes could be expressed by:

$$\frac{\sigma_{dc}}{\sigma_{op}(\lambda)} = \frac{Z_0}{2R_s}\frac{\sqrt{T}}{1-\sqrt{T}}$$

where σ_{dc} is the DC conductivity of the film, $\sigma_{op}(\lambda)$ is the optical conductivity at wavelength of λ nm, Z_0 is the impedance of free space (377 Ω), R_s is the sheet resistance, and T is the transmittance at λ nm. For industrial application, the FoM value should be larger than 35.[51] The sheet resistance plotted with FoM (black) and transmittance at 550 nm (red) is summarized in Fig. 2c. The FoM value of AgNW–PI hybrid electrodes in this work could reach 260 with high transmittance (70%) and low sheet resistance (3.6 Ω sq^{-1}). The FoM value then decreased to 250 and the sheet resistance was even enhanced to 2.7 Ω sq^{-1} due to the significant reduction of optical transmittance. Thus, the AgNW–PI hybrid film with the highest FoM value of 260 is proof that the AgNW network is dense enough to have high conductivity and transmit most optical light. The photos of the optimized AgNW–PI hybrid film are showen in Fig. 2d. To the best of our knowledge, this is the highest FoM value in a AgNW–PI hybrid system that reveals an excellent combination of optical and electric properties (as listed in Tables S4 and S5†).[52] Furthermore, the dispersion of AgNWs in the PI hybrid film was observed by SEM which is shown in Fig. 3. By taking the advantage of spraying and transferring techniques, the AgNW network could be dispersed uniformly and smoothly on the surface of PI substrates (AFM shown in Fig. S3†). In addition, no peeled track of AgNWs was found from the SEM cross-sectional view indicating strong adhesion between AgNWs and the PI binder.

Bending, peeling, and chemical resistance behavior of the flexible AgNW–PI electrodes

In order to emphasize the properties between AgNWs and PI substrates in a different harsh working environment, the bending, peeling, and chemical resistance tests of AgNW–PI

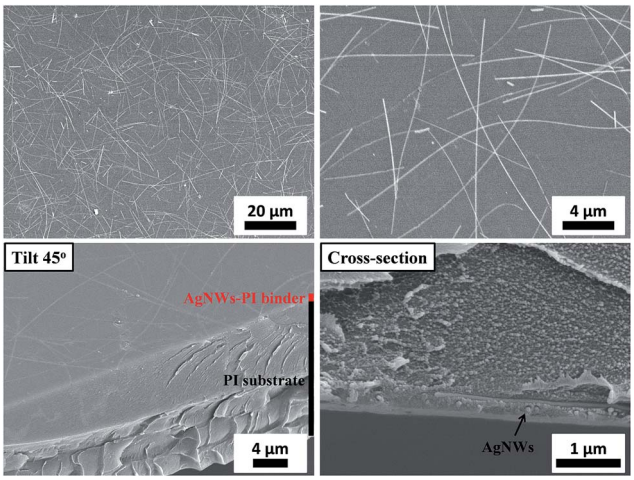

Fig. 3 SEM morphology of the AgNW–PI hybrid film.

hybrid films were investigated. The bending test fixed at a 2.5 mm radius of curvature is demonstrated in Fig. 4a and b; the AgNW–PI hybrid film with a 4.8 Ω sq^{-1} sheet resistance showed excellent ductility and stability even after bending for 10 000 cycles. On the contrary, the sheet resistance of ITO-PEN (R_s: 35 Ω sq^{-1}) exhibited considerable variation up to 100 times after bending for only 10 cycles. The sheet resistance dynamic change of the AgNW–PI hybrid film and ITO-PEN film during the bending experiment at different band angles is also depicted in Fig. S4.† Because of the excellent ductility of AgNWs, the LED light could keep working under bending and even folding conditions as shown in Fig. 4c and d.

The adhesion test of the AgNW–PI hybrid film was conducted by 3M scotch tape to confirm the protection and adhesive quality of CHDABP PI. The sheet resistance variation with peeling cycles is depicted in Fig. 5, and sheet resistance of the hybrid film could be maintained after peeling for 1000 cycles. According to the SEM observations, only very few AgNWs peeled

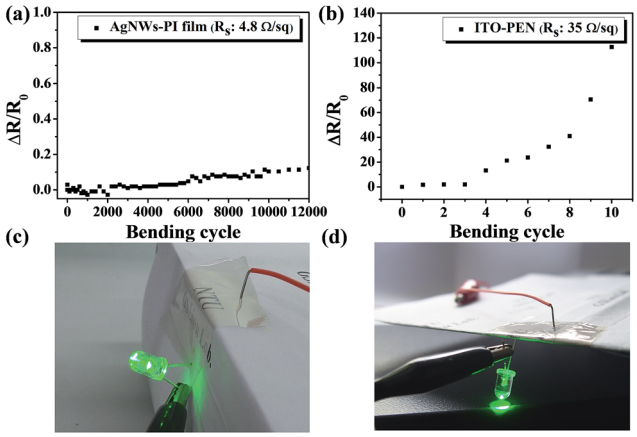

Fig. 4 Sheet resistance variation plotted with bending cycle (the radius of curvature: 5 mm) of (a) AgNW–PI hybrid film, (b) ITO-PEN film; and LED lighting demonstration of the bending AgNW–PI hybrid film at (c) 90° and (d) 180°, respectively.

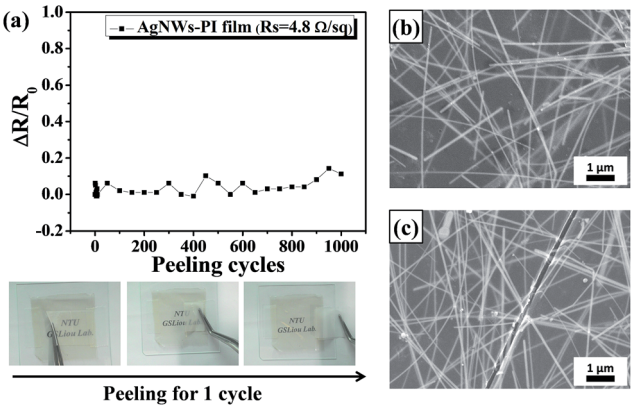

Fig. 5 (a) Peeling test of AgNW–PI hybrid film for 1000 cycles by 3M scotch tape and SEM morphology of AgNW–PI hybrid film (b) before and (c) after peeling for 1000 cycles.

off from the CHDABP PI binder compared to the reference one (without PI served as the binder) as sheet resistance increased too significantly to be measured by a 4-point probe after peeling for only 1 cycle as reported by previous work.[48]

In this AgNW–PI hybrid system, the organic-insoluble CHDABP PI which served as the binder and protector was introduced in order to improve the post-processability of the AgNW–PI electrode. Therefore, the capability of chemical resistance is crucial for practical usage. Thus, the chemical resistance test was conducted by drop-casting various organic solvents such as chloroform, acetone, THF, DMAc, NMP, DMF, and DMSO onto the surface of hybrid films. The sheet resistance variation plotted with dipping time of the hybrid films is shown in Fig. 6, and could be maintained less than 5 times even after dipping for 5.5 hours with different types of organic solvents. Furthermore, the SEM observation after dipping in organic solvents for 20 hours is summarized in Fig. S5;† the adhesion capability between AgNWs and the substrate was still maintained and only very few removed tracks of AgNWs were observed. Thus, these optically transparent and flexible AgNW–PI hybrid electrodes have extremely high potential and feasibility to operate following many kinds of post-processing.

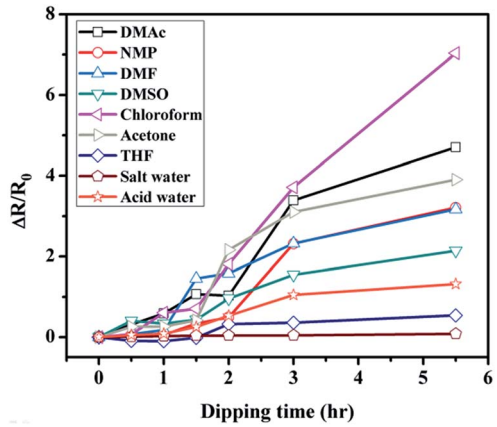

Fig. 6 Chemical resistance test of AgNW–PI hybrid films by dipping with different solvents.

Properties of the AgNW–PI heater (snow-cleaning device)

The fabricated AgNW–PI coated glass electrodes could serve as heaters at higher potential application. In order to emphasize the thermal stability and the applicability of the AgNW–PI electrode as a heating device under higher applied potential, the prepared AgNW–TFMBCH PI heating device with a sheet resistance of $6.3 \pm 0.5\ \Omega\ \mathrm{sq}^{-1}$ and transmittance ($T_{550\mathrm{nm}}$) of 76% was adopted and fixed in this study. The temperature plotted against the function of time at different applied potentials is shown in Fig. 7a (cycle time: 10 minutes). The result revealed that the saturated temperature of snow-cleaning devices is tunable by changing potentials from 3 V to 9 V according to the Joule's law described as follows:

$$Q = \frac{V^2}{R} \times t$$

where Q is the heat produced, V is the applied potential, R is the resistance of the electrode, and t is the working time. The produced heat is affected by the imported voltage and sheet resistance of the AgNW–PI electrode. The results indicated that AgNW–PI hybrids could produce higher heat when the applied potential is increased up to 9 V, and the saturated temperature reached 155 °C which reveals the importance of thermal stability of the substrate and binder in the hybrid system. For lead-acid batteries (12 V) used in automobiles, 9 V is low enough to be applied. Therefore, the AgNW–PI hybrid can serve to not only defog but also as a snow-cleaning devices.

In addition, the long-term thermal stability of heaters is an important issue for practical application. The results of the snow-cleaning device shown in Fig. 7b depict that the temperature could be maintained for more than 30 minutes at 155 °C,

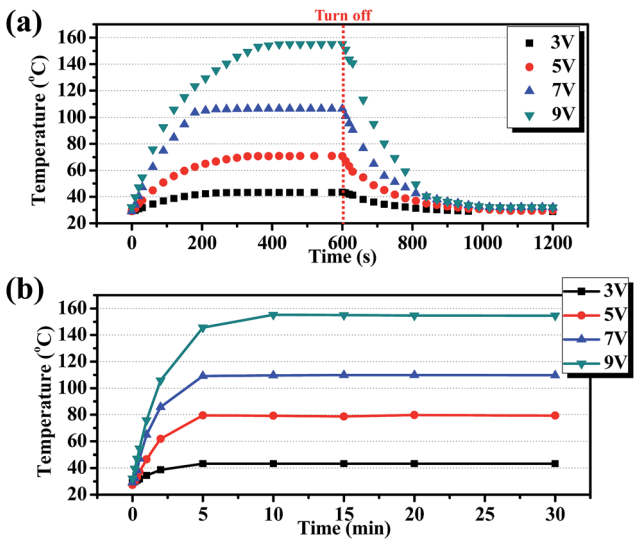

Fig. 7 (a) The temperature plotted with time at various applied potentials on the device. (b) Stability of AgNW–PI heaters at various applied potentials (surrounding temperature: 30 °C).

Fig. 8 Demonstrations of the snow-cleaning device based on AgNW–PI transparent electrode at the applied potential of 9 V (surrounding temperature: 5 °C).

and the device also simulated the real operational condition by turning on and off at a surrounding temperature of 5 °C (as shown in Fig. 8). The snow on the device was produced by the mixture of water and liquid nitrogen, and the demonstrations showed that the snow could melt into water within 1 minute at a 9 V applied potential. Thus, the AgNW–PI hybrid electrode obtained in this study reveals great advances not only in defogging but also in snow-cleaning performance.

Conclusions

In this study, highly transparent and flexible AgNW–PI hybrid films have been prepared successfully. The high aspect ratio AgNWs were also prepared by the modified polyol method, which exhibit an average diameter of 70 nm and length of 45 μm. Owing to the combination of the colorless PI substrate, the highest FoM value in the AgNW–PI research field was achieved up to 260 with a low sheet resistance of 3.6 Ω sq^{-1} and high transmittance of 70% at a 550 nm wavelength. Moreover, by introduction of high performance CHDABP PI as the protecting layer, not only the resistivity to common organic solvents but also thermal stability could be enhanced. The conductivity of these hybrid films could be maintained even after bending for 12 000 cycles and peeling for 1000 cycles. Furthermore, the AgNW–PI electrode fabricated by this system is feasible and would be a potential candidate as a snow-cleaning device even at higher temperatures up to 155 °C.

Acknowledgements

The authors are grateful to the Ministry of Science and Technology of Taiwan for the financial support.

Notes and references

1 K. Alzoubi, M. M. Hamasha, S. Lu and B. Sammakia, *J. Disp. Technol.*, 2011, **7**, 593–600.
2 S. Iijima, *Nature*, 1991, **354**, 56–58.
3 K. S. Novoselov, A. K. Geim, S. V. Morozov, D. Jiang, Y. Zhang, S. V. Dubonos, I. V. Grigorieva and A. A. Firsov, *Science*, 2004, **306**, 666–669.
4 J. Y. Lee, S. T. Connor, Y. Cui and P. Peumans, *Nano Lett.*, 2008, **8**, 689–692.
5 A. Eatemadi, H. Daraee, H. Karimkhanloo, M. Kouhi, N. Zarghami, A. Akbarzadeh, M. Abasi, Y. Hanifehpour and S. W. Joo, *Nanoscale Res. Lett.*, 2014, **9**, 393.
6 Q. Zhang, Y. A. N. Li, D. Xu and Z. Gu, *J. Mater. Sci. Lett.*, 2001, **20**, 925–927.
7 M. Saka and R. Ueda, *J. Mater. Res.*, 2011, **20**, 2712–2718.
8 Y. Sun, Y. Yin, B. T. Mayers, T. Herricks and Y. Xia, *Chem. Mater.*, 2002, **14**, 4736–4745.
9 S. De, T. M. Higgins, P. E. Lyons, E. M. Doherty, P. N. Nirmalraj, W. J. Blau, J. J. Boland and J. N. Coleman, *ACS Nano*, 2009, **3**, 1767–1774.
10 L. Hu, H. S. Kim, J. Y. Lee, P. Peumans and Y. Cui, *ACS Nano*, 2010, **4**, 2955–2963.
11 A. R. Madaria, A. Kumar, F. N. Ishikawa and C. Zhou, *Nano Res.*, 2010, **3**, 564–573.
12 P. Lee, J. Lee, H. Lee, J. Yeo, S. Hong, K. H. Nam, D. Lee, S. S. Lee and S. H. Ko, *Adv. Mater.*, 2012, **24**, 3326–3332.
13 F. Xu and Y. Zhu, *Adv. Mater.*, 2012, **24**, 5117–5122.
14 X. Ho, J. Nie Tey, W. Liu, C. Kweng Cheng and J. Wei, *J. Appl. Phys.*, 2013, **113**, 044311.
15 H. J. Lee, J. H. Hwang, K. B. Choi, S. G. Jung, K. N. Kim, Y. S. Shim, C. H. Park, Y. W. Park and B. K. Ju, *ACS Appl. Mater. Interfaces*, 2013, **5**, 10397–10403.
16 M. S. Miller, J. C. O'Kane, A. Niec, R. S. Carmichael and T. B. Carmichael, *ACS Appl. Mater. Interfaces*, 2013, **5**, 10165–10172.
17 C. Preston, Y. Xu, X. Han, J. N. Munday and L. Hu, *Nano Res.*, 2013, **6**, 461–468.
18 L. Li, Z. Yu, W. Hu, C. H. Chang, Q. Chen and Q. Pei, *Adv. Mater.*, 2011, **23**, 5563–5567.
19 Z. Yu, Q. Zhang, L. Li, Q. Chen, X. Niu, J. Liu and Q. Pei, *Adv. Mater.*, 2011, **23**, 664–668.
20 W. Hu, X. Niu, L. Li, S. Yun, Z. Yu and Q. Pei, *Nanotechnology*, 2012, **23**, 344002.
21 W. Hu, X. Niu, R. Zhao and Q. Pei, *Appl. Phys. Lett.*, 2013, **102**, 083303.
22 H.-W. Tien, S.-T. Hsiao, W.-H. Liao, Y.-H. Yu, F.-C. Lin, Y.-S. Wang, S.-M. Li and C.-C. M. Ma, *Carbon*, 2013, **58**, 198–207.
23 S. P. Chen and Y. C. Liao, *Phys. Chem. Chem. Phys.*, 2014, **16**, 19856–19860.
24 D. Lee, H. Lee, Y. Ahn, Y. Jeong, D. Y. Lee and Y. Lee, *Nanoscale*, 2013, **5**, 7750–7755.

25 K. Naito, N. Yoshinaga, E. Tsutsumi and Y. Akasaka, *Synth. Met.*, 2013, **175**, 42–46.
26 T. Kim, A. Canlier, G. H. Kim, J. Choi, M. Park and S. M. Han, *ACS Appl. Mater. Interfaces*, 2013, **5**, 788–794.
27 I. Moreno, N. Navascues, M. Arruebo, S. Irusta and J. Santamaria, *Nanotechnology*, 2013, **24**, 275603.
28 X. Y. Zeng, Q. K. Zhang, R. M. Yu and C. Z. Lu, *Adv. Mater.*, 2010, **22**, 4484–4488.
29 J. Lee, F. Sun and J. Lee, *J. Exp. Nanosci.*, 2013, **8**, 130–137.
30 S. Narayanan, J. R. Hajzus, C. E. Treacy, M. R. Bockstaller and L. M. Porter, *ECS J. Solid State Sci. Technol.*, 2014, **3**, P363–P369.
31 T. H. L. Nguyen, L. Quiroga Cortes, A. Lonjon, E. Dantras and C. Lacabanne, *J. Non-Cryst. Solids*, 2014, **385**, 34–39.
32 K.-H. Choi, J. Kim, Y.-J. Noh, S.-I. Na and H.-K. Kim, *Sol. Energy Mater. Sol. Cells*, 2013, **110**, 147–153.
33 M. Song, D. S. You, K. Lim, S. Park, S. Jung, C. S. Kim, D.-H. Kim, D.-G. Kim, J.-K. Kim, J. Park, Y.-C. Kang, J. Heo, S.-H. Jin, J. H. Park and J.-W. Kang, *Adv. Funct. Mater.*, 2013, **23**, 4177–4184.
34 S.-E. Park, S. Kim, D.-Y. Lee, E. Kim and J. Hwang, *J. Mater. Chem. A*, 2013, **1**, 14286.
35 T. C. Hauger, S. M. Al-Rafia and J. M. Buriak, *ACS Appl. Mater. Interfaces*, 2013, **5**, 12663–12671.
36 D. Y. Choi, H. W. Kang, H. J. Sung and S. S. Kim, *Nanoscale*, 2013, **5**, 977–983.
37 J. Lee, J. Y. Woo, J. T. Kim, B. Y. Lee and C. S. Han, *ACS Appl. Mater. Interfaces*, 2014, **6**, 10974–10980.
38 S. Coskun, E. Selen Ates and H. E. Unalan, *Nanotechnology*, 2013, **24**, 125202.
39 J. Lee, P. Lee, H. Lee, D. Lee, S. S. Lee and S. H. Ko, *Nanoscale*, 2012, **4**, 6408–6414.
40 A. R. Madaria, A. Kumar and C. Zhou, *Nanotechnology*, 2011, **22**, 245201.
41 D. Kim, L. Zhu, D.-J. Jeong, K. Chun, Y.-Y. Bang, S.-R. Kim, J.-H. Kim and S.-K. Oh, *Carbon*, 2013, **63**, 530–536.
42 T. Kim, Y. W. Kim, H. S. Lee, H. Kim, W. S. Yang and K. S. Suh, *Adv. Funct. Mater.*, 2013, **23**, 1250–1255.
43 R. Gupta, K. D. Rao, K. Srivastava, A. Kumar, S. Kiruthika and G. U. Kulkarni, *ACS Appl. Mater. Interfaces*, 2014, **6**, 13688–13696.
44 S. Ji, W. He, K. Wang, Y. Ran and C. Ye, *Small*, 2014, **10**, 4951–4960.
45 J. Li, J. Liang, X. Jian, W. Hu, J. Li and Q. Pei, *Macromol. Mater. Eng.*, 2014, **299**, 1403–1409.
46 S. Sorel, D. Bellet and J. N. Coleman, *ACS Nano*, 2014, **8**, 4805–4814.
47 X. Zhang, X. Yan, J. Chen and J. Zhao, *Carbon*, 2014, **69**, 437–443.
48 H.-Y. Lu, C.-Y. Chou, J.-H. Wu, J.-J. Lin and G.-S. Liou, *J. Mater. Chem. C*, 2015, **3**, 3629–3635.
49 K. E. Korte, S. E. Skrabalak and Y. Xia, *J. Mater. Chem.*, 2008, **18**, 437–441.
50 G. Haacke, *J. Appl. Phys.*, 1976, **47**, 4086.
51 S. Sorel, P. E. Lyons, S. De, J. C. Dickerson and J. N. Coleman, *Nanotechnology*, 2012, **23**, 185201.
52 C.-Y. Chou, Master's thesis, National Taiwan University, 2015.

